NOVEL EQUIMOLAR MEDIUM ENTROPY ALLOY (TI-W-MO) VIA SELECTIVE LASER MELTING FOR HIGH TEMPERATURE APPLICATIONS

A Thesis

by

LINDSEY SALAZAR

Submitted in Partial Fulfillment of the

Requirements for the Degree of

MASTER OF SCIENCE

Major Subject: Engineering Management

The University of Texas Rio Grande Valley

June 2024

NOVEL EQUIMOLAR MEDIUM ENTROPY ALLOY (TI-W-MO) VIA SELECTIVE LASER MELTING FOR HIGH TEMPERATURE APPLICATIONS

A Thesis
by
LINDSEY SALAZAR

COMMITTEE MEMBERS

Dr. Jianzhi Li
Chair of Committee

Dr. Farid Ahmed
Committee Member

Dr. Yangyang Long
Committee Member

Dr. Brandon McWilliams
Committee Member

June 2024

ABSTRACT

Salazar, Lindsey, Novel Equimolar Medium Entropy Alloy (Ti-W-Mo) Via Selective Laser Melting for High Temperature Applications. Master of Science (MS), June 2024, 29 pp., 14 figures, 30 references.

High-temperature strength and high environmental resistance are necessary characteristics for materials under extreme working conditions in aerospace, nuclear, and chemical industries. In this study, a novel refractory medium entropy alloy (MEA) was developed from tungsten (W), titanium (Ti), and molybdenum (Mo) via an additive manufacturing process, selective laser melting (SLM). Through process optimization, (i) the formation of brittle intermediate phases was suppressed, (ii) the complete melting of tungsten particles was achieved, and (iii) a pure solid solution was formed. Due to the addition of Ti and Mo, the resultant alloy showed outstanding high-temperature strength compared to other tungsten alloys. The effects of process parameters on the mechanical properties were analyzed to understand the characteristics of complex layer-by-layer structures. The feasibility of manufacturing defect-less refractory MEA composed of a solid solution phase delivers high potentials of laser-based additive manufacturing in functional material development.

DEDICATION

This thesis is dedicated to my family and fiancé Hernan Aparicio for their love, understanding, and support at this challenging point in my life. I would especially want to thank my father, Carlos Salazar, and mother, Norika Lucio-Salazar, for making sacrifices throughout their lives to build a brighter future for my sister and myself. Finally, I want to thank my heavenly father for leading me through this incredible experience.

ACKNOWLEDGMENTS

I would like to extend my sincere appreciation to Dr. Tarawneh and CREST for his support throughout my degree, as well as Dr. Jianzhi Li and Dr. Farid Ahmed, my mentors, for their invaluable guidance throughout the duration of this research. The work presented in this thesis was funded by the NSF CREST Center for Multidisciplinary Research Excellence in Cyber-Physical Infrastructure Systems (MECIS) under NSF Award No. 2112650.

I am especially grateful to Dr. Jeongwoo Lee for his outstanding advice, which has significantly contributed to my development as a more objective researcher during the course of this study.

A sincere thank you to Angela Scardigno, Oscar Martinez, Dr. Victoria Padilla, Dr. Jefferson Reinoza, Mr. Marcos Villarreal, and Mr. Bryan Hoke for their roles as colleagues, friends, staff, and for graciously allowing me the use of their equipment for analysis.

TABLE OF CONTENTS

Page

LIST OF FIGURES

Page

CHAPTER I

INTRODUCTION

High entropy alloys (HEAs) are a composition of three or more principal elements where each element should have a concentration between 5 and 35 at. %. These alloys are named HEAs because the random solid solution states have higher mixing entropy compared to conventional alloys. Additionally, HEAs are alloys with an entropy of (SSS, ideal > 1.61R, where SSS, ideal is the total configurational molar entropy in an ideal solid solution (SS) and R is the gas constant), medium (0.69 < SSS, ideal < 1.61R) and low SSS, ideal < 0.61R). [16] Specifically, a medium entropy alloy (MEA) refers to an alloy formed by the melting of 2 to 4 elements with an equal atomic ratio, and the structural entropy is between 1 and 1.5 R as previously explained. [25] Because of the variety of principal elements that are used to create a HEA, unique characteristics can form. These involve high strength/hardness, outstanding wear resistance, exceptional high-temperature strength, good structural stability, good corrosion, and oxidation resistance. These characteristics have exceeded the ones from conventional alloys, making these alloys attractive to different fields of research and its application range is considerably more broadened by the fact that it may be employed at high temperatures. Some of the applications of HEAs can surpass the capabilities of nickel-based superalloys and these include high temperature superalloy components in aerospace propulsion systems, land-based gas turbines, nuclear reactors, heat exchanging tubing, chemical process industry and among others. [21] After mentioning the benefits of HEAs, it's necessary to discuss some of the challenges about manufacturing them. HEAs can be difficult to work with because of its four core effects, the high entropy effect, the lattice distortion effect, the sluggish diffusion effect, and the 'cocktail' effect. [22] These core effects need to be taken into consideration when a novel material is being developed, as well as the mechanical properties of each element in

the composition, such as the hardness and melting temperature. These properties are critical because the development of a material containing refractory metals, for example, could be impossible to fabricate using conventional manufacturing techniques. For this reason, researchers have been looking for advanced technologies that meet the criteria for the advancement of new high, medium, or low entropy alloys. To mitigate this problem, selective laser melting (SLM) has been shown to be superior to other processes (e.g., SPS) because of its tensile strength, yield strength, and elongation. The reason for its superiority is the excellent metallurgy bonding, multiple-scale grains, dispersed precipitations, finer grains, and stronger texture that the process contributes, and the ability to reach high melting temperatures which can elevate the mechanical properties of different materials. For these reasons, this process emerges as a promising candidate for developing High Entropy Alloys (HEAs) [22], as well as the incorporation of in-situ sensors and cameras to further enhance the potential to produce high-quality parts. [11] Among various HEAs, refractory HEAs and MEAs are deemed particularly well-suited for applications in elevated temperature environments. This includes applications like high temperature heat exchangers for power plants, where temperatures exceed 650 degrees Celsius [1], as well as gas turbines typically exposed to temperatures surpassing 730 degrees Celsius. [15] Refractory HEAs exhibit exceptional oxidation resistance, a vital property at high temperatures, attributed to specific alloying elements such as titanium. Making them particularly advantageous for aerospace and energy applications. [17] Since one of the several advantages of SLM is the high melting points the process can reach and the need for materials that can withstand extreme temperatures, studies on HEAs that include titanium (Ti), molybdenum (Mo), and tungsten (W) in their composition have been investigated due to its exceptional contributions in different compositions. The addition of titanium (Ti) was observed to be key in the gamma phase formation which increases the strength and ductility in a mixture, tungsten was observed to increase the strength, beta-Ti phase stability, and WMo was observed to increase tensile strength on the material [14], [9], [27], [20], [13], [3]. Although there have been studies that show the consolidation of alloys containing Ti, Mo, and W, there are limited studies that explore a medium entropy alloy with only these three elements and most of the articles have not

been able to create a homogeneous composition with the addition of W. Sintered Ti80Mo10W10 and Ti90Mo5W5 [4] showed an inhomogeneous composition. [3] showed unmelted particles of tungsten and molybdenum which makes a non-homogeneous microstructure and caused crack formation. In this study, the development of a new refractory medium entropy alloy, TiWMo, is going to be created and different set of parameters are going to be employed to investigate how they affect the composition homogeneity, microstructure, and mechanical properties of the material.

1.1 Problem Statement

The challenge at hand involves the fabrication of a medium entropy alloy, specifically an equimolar combination of titanium, molybdenum, and tungsten (Ti-Mo-W), for applications demanding elevated temperature resistance. Traditional manufacturing techniques are rendered impractical due to the exceptionally high melting points of tungsten, molybdenum, and titanium. In response, selective laser melting, an additive manufacturing method, is proposed for its efficacy in handling materials with formidable melting points. However, a formidable obstacle arises in the development process, particularly concerning tungsten, given its exceptionally high melting point of 3422 degrees Celsius, posing difficulties in achieving a homogeneous microstructure essential for the alloy's optimal performance. This predicament underscores the central problem: the need to overcome the challenges associated with the creation of a homogeneous microstructure in a medium entropy alloy with constituents boasting exceptionally high melting points.

1.2 Research Objectives

1. Examine the production process of the medium entropy alloy TiMoW utilizing selective laser melting. 2. Assess the influence of laser parameters on the constituent powder composition. 3. Conduct high-temperature testing of the material within a furnace. 4. Examine the alloy's microstructure both prior to and following exposure to elevated temperatures. 5. Evaluate the mechanical characteristics of the TiMoW medium entropy alloy after exposure.

1.3 Experimental Design and Methods

To complete the fabrication of the TiMoW medium entropy alloy was the following, elemental powder of titanium, tungsten, and molybdenum was sieved using a 60-um sieve specifically for tungsten and molybdenum. Based on previous findings, titanium and molybdenum were able to melt through selective laser melting. Specifically for tungsten, a sieve of less than or equal to 35 um was used. A study found that by using a lower particle size the powder was able to melt and diffuse together more easily compared to higher particle sizes. For particles with a diameter of 5 um, the absorptivity of the powder layer reached a maximum value of 0.6030. This value dropped slightly to 0.6028 for a particle diameter of 15 um, indicating that the diameter of the particles has a slight effect on absorption when the particle size is less than 15 um. With a further increase in particle size to 25 um, the powder layer absorptivity diminished dramatically to 0.5615 [29]. The powder was mixed using a V-mixer with at one revolution per second. A combination of parameters which include laser power, hatch distance, scanning speed, and layer thickness was applied in an attempt to fabricate four samples on a titanium plate. After completing the prints, they were analyzed using scanning electron microscopy (SEM) to observe any defect formation on the print and unmelted particles. Energy dispersive microscopy (EDS) was used to observe what was the composition throughout the sample, and powder X-ray diffraction (XRD) was used to determine which phases formed on the composition. As part of the future work, it has been planned that eight samples are going to be printed using the same laser parameters, but with a tungsten particle size of less than or equal to 25 microns. The samples are going to be exposed to elevated temperatures in a furnace and the microstructure of the alloy prior to exposure and after exposure is going to be analyzed through SEM and EDS. The tensile strength and microhardness of the material are going to be tested after they have been exposed to high temperatures to observe their performance under extreme conditions.

CHAPTER II

LITERATURE REVIEW

2.1 Application of Medium Entropy Alloys

Some of the properties of high entropy alloys include sound hardness, excellent corrosion resistance [13], and high temperature resistance [21]. The popularity of high and medium entropy alloys has been increasing in the last years because they have been found to have superior mechanical properties compared to RHEAs made by casting [13] and nickel-based super alloys [21]. Some of the applications where refractory high entropy alloys include are high temperature superalloy components in aerospace propulsion systems, land-based gas turbines, nuclear reactors, heat exchanger tubing, and the chemical process industry, rocket engine nozzles, and rotating anodes for X-ray production [21]. The majority of HEAs exploration efforts currently seek to surpass requirements of the most demanding superalloy applications—blades, vanes, and disks in aerospace gas turbine engines. These applications require a range of physical and mechanical properties. Foremost is the combination of both high temperature tensile strength and sufficient damage tolerance to resist failure during assembly (i.e., at RT) and operation. Of these components, blades and vanes operate at the highest temperatures (900–1000 °C), and the tensile strengths of commercial superalloy cast, single-crystal blade materials are in the range of 200–500 MPa at 980 °C [21].

2.2 Microstructure of Medium Entropy Alloys

Medium entropy alloys (MEAs) are composed of three or four principal elements in nearly equiatomic proportions. The microstructure of MEAs is diverse and unique, depending on the specific elements, their atomic percentages, and the processing methods employed. Several key

characteristics of MEAs include: Phase Composition Many MEAs form a single-phase solid solution, either body-centered cubic (BCC) or face-centered cubic (FCC). This single-phase structure is stabilized by the high entropy of mixing, which enhances the solubility of different elements in the alloy. However, some MEAs may also exhibit multi-phase structures, depending on the elements and processing conditions. Grain Structure The grain structure of MEAs varies widely based on cooling rates and processing techniques. Fine-grained structures are often preferred due to their enhanced mechanical properties, such as increased strength and toughness. Grain boundaries in MEAs play a significant role in determining the material's properties. Due to the presence of multiple principal elements, these grain boundaries are often more complex than those found in traditional alloys, affecting strength and ductility. Elemental Distribution Ideally, each element in an MEA would be uniformly distributed throughout the solid solution to achieve optimal properties. However, in practice, slight segregation or clustering of elements can occur, especially in multi-phase MEAs. At the atomic scale, MEAs exhibit significant lattice distortions due to the varying atomic sizes of the constituent elements. These distortions can influence dislocation movement, thereby impacting the mechanical properties of the alloy. Influence on Mechanical Properties The microstructure of MEAs is crucial in determining their mechanical properties. By carefully controlling the alloy composition and processing conditions, it is possible to tailor these properties for specific applications. For instance, optimizing the grain size and distribution can enhance strength and ductility, while managing phase composition can improve thermal stability and resistance to deformation. Additional Characteristics MEAs can also form various precipitates and secondary phases, which contribute to strengthening mechanisms such as precipitation hardening. These secondary phases can include carbides, nitrides, or intermetallic compounds, depending on the specific alloy system. Furthermore, the presence of mechanical twins and unique dislocation structures can significantly affect the material's response to deformation, providing a balance between strength and ductility. Overall, the microstructure of medium entropy alloys is a critical factor in their performance. Careful design and processing of MEAs allow for the optimization of their properties, making them suitable for a wide range of advanced applications, from structural

components to high-temperature environments [19], [28], [12], [16], [25], [26], [30].

2.3 Mechanical Properties of Medium Entropy Alloys

Medium entropy alloys (MEAs) are characterized by a range of exceptional mechanical properties. They exhibit remarkable high strength and tensile strength, allowing them to withstand significant loads and stresses. Additionally, MEAs possess excellent ductility, enabling them to undergo substantial deformation without fracturing. This is complemented by their significant elongation, which means they can stretch considerably before breaking. The hardness of MEAs is notably high, contributing to their excellent wear resistance, making them suitable for applications where durability is critical. These alloys also demonstrate high fracture toughness, which ensures they can resist crack propagation and failure under stress. Furthermore, MEAs have commendable fatigue properties, allowing them to endure repeated cyclic loading without succumbing to fatigue failure. Their creep strength is another notable attribute, maintaining their structural integrity under prolonged exposure to high temperatures and stresses. One of the standout features of MEAs is their stable mechanical properties at elevated temperatures, making them reliable for use in high-temperature environments. They also exhibit enhanced strain hardening, where the material becomes stronger and more resistant to deformation with continued use. Overall, the superior combination of these properties makes medium entropy alloys a highly valuable class of materials for a wide range of demanding applications [7], [24], [25], [26], [30] [6], [18].

2.4 Laser Powder Bed Fusion and Processing Parameters

According to the existing literature, selective laser melting (SLM) demonstrates superiority in terms of tensile strength, yield strength, and elongation. This superiority can be attributed to the exceptional metallurgical bonding, multiple-scale grains, dispersed precipitations, finer grains, and stronger texture facilitated by the SLM process [26]. Consequently, SLM, as a representative additive manufacturing (AM) technology, is extensively utilized in shaping metals with intricate structures, showcasing high precision in applications like high-entropy alloys, silicon brass alloys, and Al-SiMg alloys [30]. The recent advancements in AM equipment, part quality, increased

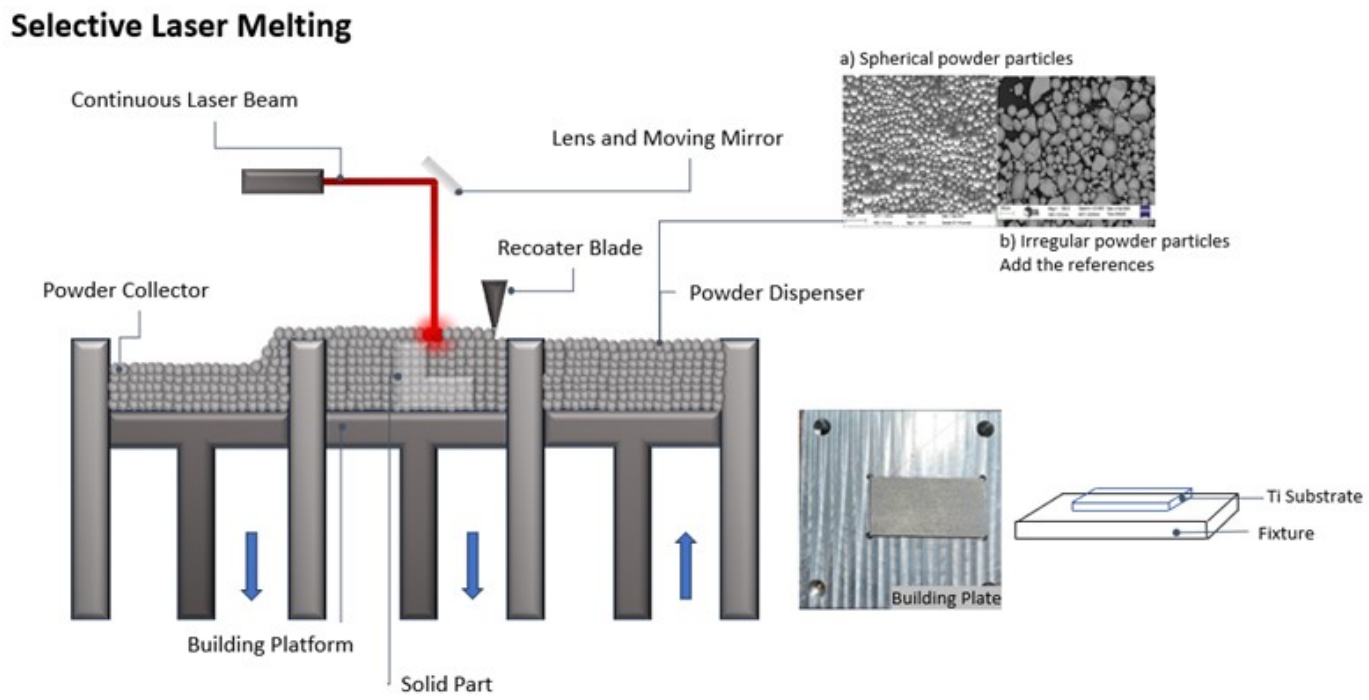

Figure 2.1: Schematic of the selective laser melting process (SLM). a) Scanning electron microscopy (SEM) of spherical powder particles and, b) SEM of irregular powder particles.

flexibility regarding part geometry, growing demand for personalized production, reduced material wastage, and energy efficiency contribute to the numerous advantages of AM. This has led to a surge in popularity, with a projected material sales increase to $9 billion by 2026 [8]. The evolution of the term "3D printing" within the AM technical community encompasses all low-cost AM fabricators, irrespective of the fabrication technique, starting from the MIT binder jetting process [2]. The direct production from 3D CAD models eliminates the need for tools and molds, resulting in cost savings with no switch-over costs. Digital file-based designs can be easily shared, facilitating modification and customization of components and products. The additive nature of the process not only saves materials but also allows for the reuse of waste materials (e.g., powder, resin), with estimated recyclability rates ranging from 95% to 98% for metal powders. Technology enables the creation of novel, intricate structures like free-form enclosed structures, channels, and lattices. Final parts exhibit minimal porosity, and the make-to-order approach reduces inventory risk, eliminating unsold finished goods. Additionally, revenue flow improves as payment is received before manufacturing begins [5].

2.5 Research Gap

One of the several advantages of Selective Laser Melting (SLM) is its ability to achieve high melting points, which is crucial for processing materials that must withstand extreme temperatures. Consequently, studies on medium entropy alloys (MEAs) and high entropy alloys (HEAs) that incorporate titanium (Ti), molybdenum (Mo), and tungsten (W) have been conducted due to their exceptional contributions in various compositions. The inclusion of titanium has been found to be essential for gamma phase formation, which enhances the strength and ductility of the alloy. Tungsten increases strength and beta-Ti phase stability, while the combination of W and Mo enhances tensile strength [14], [9], [27], [20], [13], [3]. Despite studies on the consolidation of alloys containing Ti, Mo, and W, there is limited research specifically on medium entropy alloys composed solely of these three elements. Most studies have struggled to achieve a homogeneous composition when adding tungsten. For instance, sintered Ti80Mo10W10 and Ti90Mo5W5 alloys displayed inhomogeneous compositions [4], and another study reported the presence of unmelted tungsten and molybdenum particles, leading to a non-homogeneous microstructure and crack formation [3]. Therefore, this study aims to develop a new refractory medium entropy alloy, TiWMo. Different sets of parameters will be employed to investigate their effects on composition homogeneity, microstructure, and mechanical properties of the material.

CHAPTER III

METHODOLOGY

3.1 Element Selection

The selection of the elements to compose the alloy have been selected based on the purpose of the material, which is to use the alloy for high temperature applications; these elements are titanium, molybdenum, and tungsten. After conducting literature review, it has been found that titanium is key in the gamma phase formation and this phase increases strength of the alloy without compromising the ductility of the composition. Also, the addition of tungsten and molybdenum (WMo) was observed to improve the tensile properties and strength of CoCrFeNi [14].

[9] this article states that their goal is to increase the plasticity of NbMoTaW and VNbMoTaW HEAs. They developed TiNbMoTaW HEA and investigated the impact of adding titanium on the structural stability and mechcanical properties at both room and elevated temperatures. The results showed the both HEAs possessed BCC structures by adding titanium to the mixture, the strength increased, as well as the ductility. The authors concluded that the addition of titanium can be interpreted in terms of solid solution hardening model. Both HEAs exhibited yield strengths higher than 550 MPa at 1200 Celsius. The high-temperature mechanical performance of these two HEAs makes them to be potential materials for high-temperature applications.

Another study created a single phased nanocrystalline refractory VNbMoTaW HEA, the powder for this alloy was produced by mechanical alloying and it was found that the alloy structure was BCC structure as well as a maximum hardness of 11.4 GPa [27].

3.2 Powder Composition and Mixing

This medium entropy alloy (MEA) is composed of titanium, molybdenum, and tungsten in an equiatomic ratio, ensuring each element constitutes 33 atomic percent. This composition meets the MEA criteria, which stipulate that the alloy must consist of 2 to 4 elements, each with equal atomic percentages. Each element underwent sieving to achieve the precise and desired powder size. Titanium powder exhibits a spherical morphology with particle sizes ranging from 15 to 45 microns. Similarly, molybdenum powder also has a spherical morphology with a particle size of 45 microns. To compare the material's microstructure with varying tungsten particle sizes and morphologies, three distinct prints were produced. For the first print, tungsten was sieved to obtain spherical particles of 45 microns. The second print utilized irregular particles of 32 microns, and the third print employed irregular particles ranging from 5 to 25 microns, as detailed in Figure 3.1. Research indicates that tungsten particles smaller than 25 microns significantly enhance laser absorptivity, facilitating easier melting and resulting in a more homogeneous microstructure [29]. After sieving, each element was accurately weighed to ensure a 33 atomic percent composition and then mixed using a V-mixing machine for 15 hours to achieve a uniform blend.

3.3 Sample Fabrication

The fabrication of the samples was done through selective laser melting using the 3D printer EOS M290. Four prints were created with different set of parameters (L), varying laser power and scanning speed, but a fixed hatch distance of 0.1 mm and a layer thickness of 0.05 mm Figure 3.1. Print 1 (L1) was created using a laser power of 350 watts and a scanning speed of 380 mm/s, print 2 (L2) was created with a laser power of 350 watts and a scanning speed of 250 mm/s, print 3 (L3) was created with a laser power of 380 watts and a scanning speed of 250 mm/s, and print 4 (L4) was created with a laser power of 280 watts and a scanning speed of 380 mm/s. The preparation of the sample for testing is shown in Figure 3.2, the samples where first cut using a diamond cutter from the titanium substrate, the second step was to mount the samples using cold mounting with epoxy and resin, the third step was to polish the samples manually, the fourth and last step was to mirror

Parameter name	Laser power P (W)	Scanning speed V (mm/s)	Hatch distance h (mm)	Layer thickness t (mm)	Energy density $\frac{P}{Vht}(J/mm^3)$
L1	350	380	0.1	0.05	184.21
L2	350	250	0.1	0.05	280
L3	280	250	0.1	0.05	224
L4	280	380	0.1	0.05	147.37

Parameter name	Substrate material	Composition	Manufacturer / Vendor
S1	Steel	Fe ~ 99%	EOS
S2	Tungsten	W 99%	McMaster
S3	Titanium	Ti 99 %	McMaster

Parameter name	Tungsten Powder	Titanium Powder	Molybdenum Powder
	Morphology/ Size	Morphology/ Size	Morphology/ Size
P1	Spherical/ 45um	Spherical/ 15-45um	Spherical/ 45um
P2	Irregular/ 32um	Spherical/ 15-45um	Spherical/ 45um
P3	Irregular/ 5-25um	Spherical/ 15-45um	Spherical/ 45um

Figure 3.1: Fabrication parameter table composed of the laser parameters used to fabricate each sample, the type of substrate used in each experiment, and the powder used to print all samples.

polish the samples to prepare them for SEM and microhardness. The fabrication of the samples was accomplished through selective laser melting using the EOS M290 3D printer. Four distinct samples were produced, each with a unique set of laser parameters (L), varying in laser power and scanning speed, while maintaining a constant hatch distance of 0.1 mm and a layer thickness of 0.05 mm as listed in Figure. 3.1. Sample 1 (L1) employed a laser power of 350 watts and a scanning speed of 380 mm/s. sample 2 (L2) utilized a laser power of 350 watts and a scanning speed of 250 mm/s. sample 3 (L3) was fabricated with a laser power of 380 watts and a scanning speed of 250 mm/s, and sample 4 (L4) was created using a laser power of 280 watts and a scanning speed of 380 mm/s. The sample preparation process for testing is illustrated in Figure 3.2. Initially, the samples were sectioned from the titanium substrate using a diamond cutter. Subsequently, the samples were mounted using cold mounting techniques with epoxy and resin. Following this, the samples underwent manual polishing. The final step involved mirror polishing to prepare the samples for Scanning Electron Microscopy (SEM) and microhardness testing.

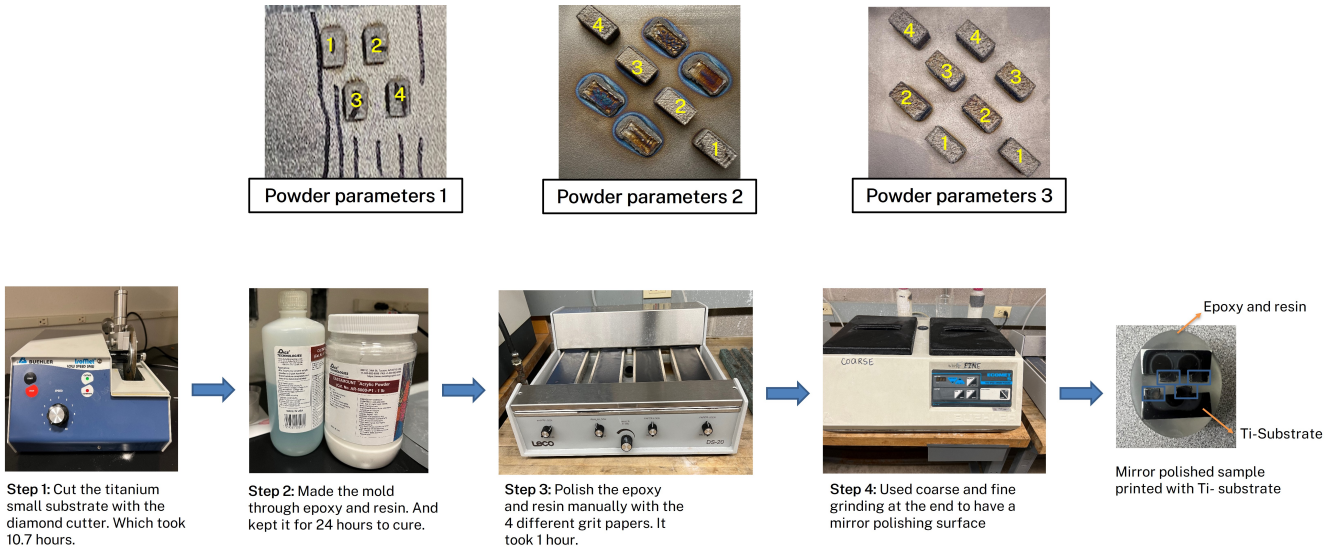

Figure 3.2: Sample fabrication steps used for scanning electron microscopy (SEM) analysis and microhardness testing and analysis at room temperature.

3.4 Testing

The samples were subjected to comprehensive testing using Scanning Electron Microscopy (SEM), X-ray Diffraction (XRD), and microhardness assessments. The SEM analysis was performed to verify the achievement of a homogeneous microstructure and to evaluate the influence of varying laser parameters and particle sizes on the samples' microstructural characteristics. The XRD analysis was conducted to identify and quantify the phases present within the material composition. Microhardness testing was carried out at ambient temperature to assess the material's performance under these conditions and to establish a baseline for future comparisons with its microhardness when exposed to elevated temperatures, relevant for high-temperature applications. These analyses provide critical insights into the material's structural integrity and phase composition, ensuring its suitability for advanced engineering applications. The SEM analysis helps in understanding the distribution and morphology of the particles within the matrix, which is crucial for predicting the material's behavior under different operational conditions. The XRD analysis reveals the crystallographic structure and potential phase transformations, which are essential for determining the material's thermal stability and mechanical properties. Microhardness testing at room temperature

serves as a preliminary evaluation of the material's hardness, which will be compared against data obtained from high-temperature testing to assess any degradation or enhancement in performance due to thermal exposure.

CHAPTER IV

RESULTS

4.1 Powder Flowability Test

The flowability of each powder was tested manually using the EOS M290 3D printer with a layer thickness of 50 microns. This procedure aimed to accurately assess the flowability and provide a reference for how the powder would behave during the printing process. Figure 4.1 illustrates that titanium (Ti) and molybdenum (Mo) exhibited good flowability, whereas tungsten (W) demonstrated poor flowability, forming clumps immediately after sieving. To address this issue, the W powder was mixed in a V-shape mixer with small steel balls for 15 hours. Although this process improved the flowability, clumps persisted. To further enhance the flowability, the W powder was then mixed with silica balls for an additional 15 hours to absorb any residual moisture. After these preliminary treatments, all the elements were mixed together in a V-mixer machine for 15 to 20 hours. Figure 4.2 shows the improved flowability of TiWMo powders: (a) with W particle sizes between 25 μm and 32 μm, and (b) with W particle sizes of 25 μm or less, both at a layer thickness of 50 μm. Testing the flowability of the powder before printing is crucial to ensure an even powder flow during the printing process. Better flowability leads to higher quality parts, as it helps prevent the formation of pores and cracks. This is essential for achieving the desired mechanical properties and structural integrity in the final printed components.

4.2 Microstructure and EDS analysis of TiMoW

In Figure 4.3, it is evident that using an energy density of 184.21 J/mm³ resulted in some tungsten particles not being fully melted, a phenomenon observed across all four laser parameters. The percentage of unmelted tungsten in the microstructure was quantified using ImageJ and

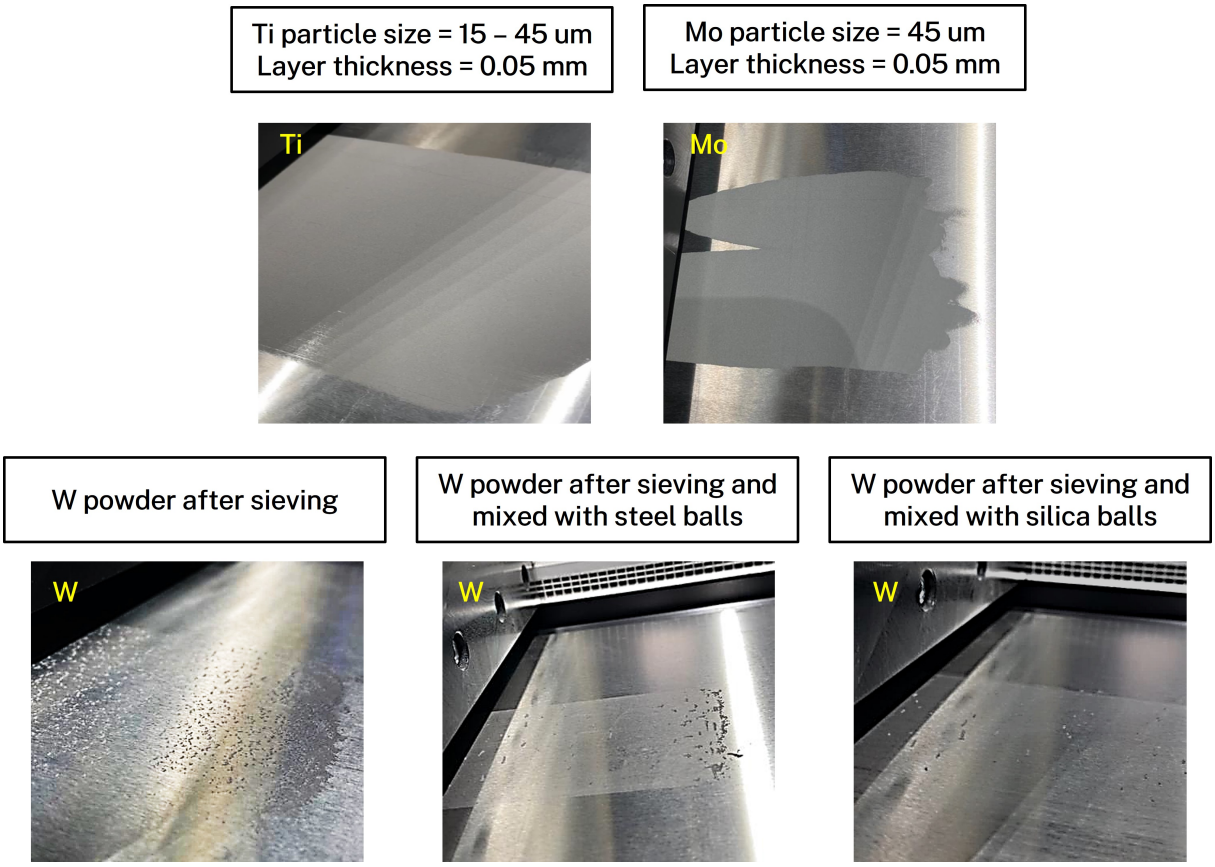

Figure 4.1: Flowability test in EOS M290 of titanium (Ti), molybdenum (Mo), and tungsten (W) with a layer thickness of 50 microns.

MATLAB for increased accuracy. The analysis revealed that with an energy density of 280 J/mm³, the percentage of unmelted tungsten in the sample's cross-section center was 0.88%, whereas, with an energy density of 224 J/mm³, it was 2.84%, and with 147.37 J/mm³, it was 1.59%. Thus, applying an energy density of 280 J/mm³ significantly reduced the percentage of unmelted tungsten to 0.88% compared to the other three samples.

Similar observations were made with sample group two in Figure 4.4 and sample group three in Figure 4.5. In group two, the percentage of unmelted tungsten decreased to 0.49% with an energy density of 280 J/mm³, and in group three, it further decreased to 0.01% with the same energy density. Additionally, comparing the unmelted tungsten percentages across the three groups, a decreasing trend is observed from group one to group three. This trend is attributed to the reduction in tungsten powder particle size and morphology from 45 microns to 25 microns or less. Consequently, smaller

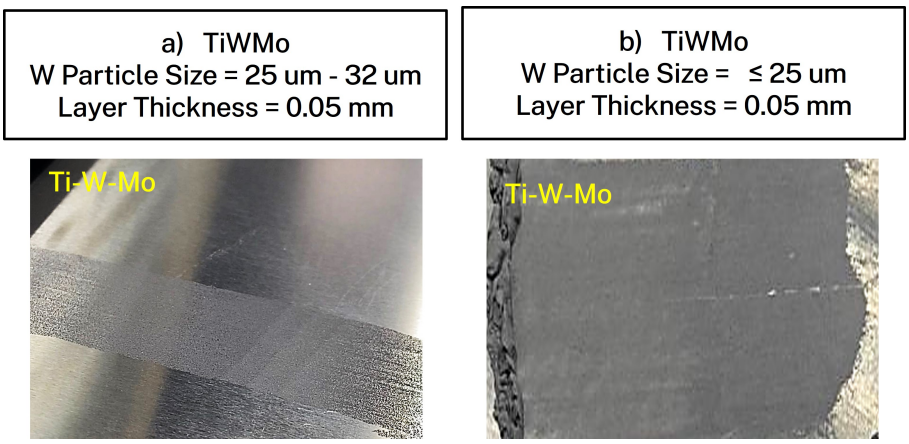

Figure 4.2: Flowability of TiWMo in EOS M290 with a layer thickness of 50 microns using varying tungsten particle size of a) 25 microns - 32 microns, and b) less than or equal to 25 microns.

particle size and irregular morphology, combined with an energy density of 280 J/mm³, result in a significant reduction in the percentage of unmelted tungsten as seen in Figure 4.6.

In Figure 4.7, Energy Dispersive Spectroscopy (EDS) was used to measure the atomic composition from the bottom to the top of the sample. The material composition (TiWMo) stabilizes at approximately 33 atomic percent at a height of 1 mm. This indicates that the powder sieving, mixing, flowability, and fabrication using the Laser Powder Bed Fusion (LPBF) process were accurately executed. Furthermore, EDS mapping of sample 3 - group 3, which had the least amount of unmelted tungsten, revealed varying microstructure shapes and sizes, indicating higher atomic percentages of certain elements. The mapping analysis identified regions rich in tungsten, tungsten-molybdenum, and tungsten-titanium, with different colors used to distinguish these elements in the microstructure. Overall, the composition is predominantly homogeneous, with an even distribution of all three components throughout the microstructure.

4.3 Phase Prediction and XRD Analysis of TiMoW

Regarding the phase prediction of the Ti-W-Mo alloy, we can theoretically determine the phase formation by calculating the valence electron concentration (VEC), thermodynamic parameters, and the enthalpy of mixing, which are listed in Figure 4.8 [23], [10].

A VEC greater than or equal to 8 typically predicts an FCC phase solid solution, while a

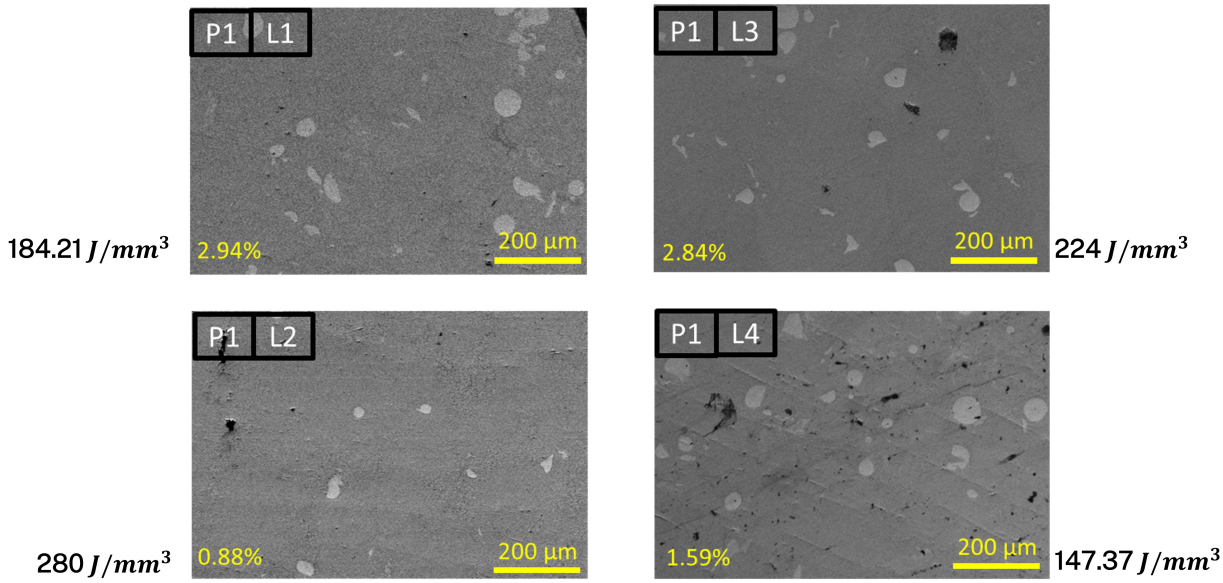

Figure 4.3: SEM of sample group 1. The white areas are unmelted tungsten and the energy density is listed as well as the unmelted tungsten percentage.

VEC less than 6.87 predicts a BCC phase solid solution. For the Ti-W-Mo alloy, the calculated VEC is 5.28, indicating a high likelihood of forming a BCC phase.

To further support this prediction, the thermodynamic parameter should be greater than or equal to 1.1. Our calculated value is 1.9, reinforcing the possibility of developing a BCC phase. Additionally, a more negative enthalpy of mixing suggests that the elements mix well, increasing the likelihood of a stable BCC phase.

Given these points, we anticipate a stable BCC phase formation. The relatively small differences in electronegativity among the elements favor the formation of a solid solution. Moreover, a smaller atomic size difference promotes the formation of a single-phase solid solution, such as BCC [23], [10].

To confirm this experimentally, XRD analysis was performed on various samples printed with different laser parameters, and all showed consistent peaks, proving the presence of a BCC phase as seen in Figure 4.9.

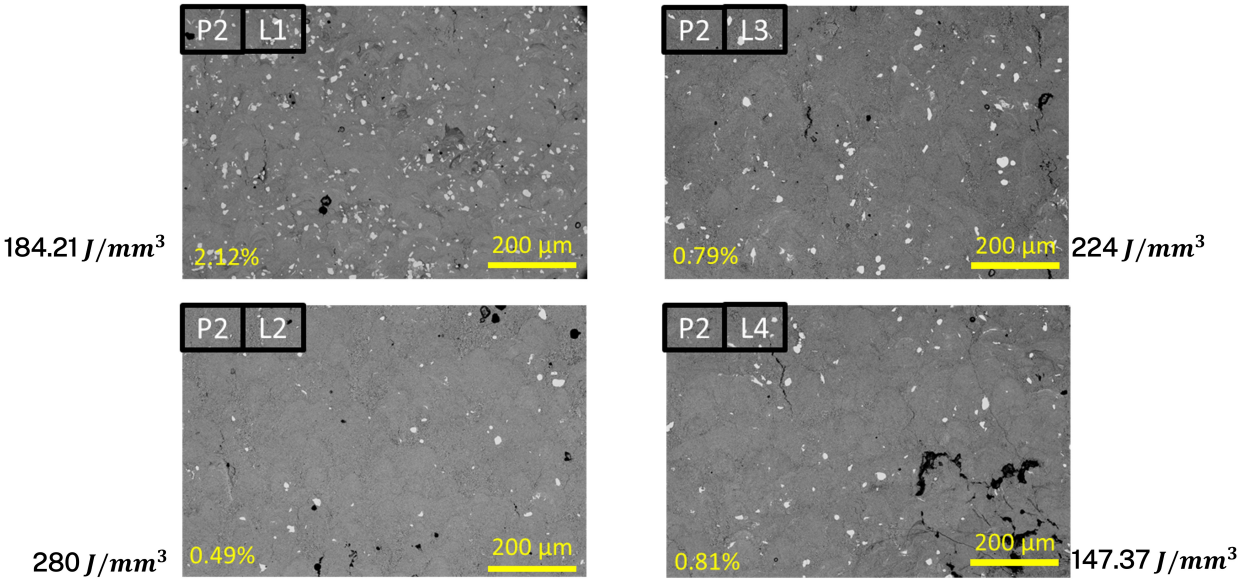

Figure 4.4: SEM of sample group 2. The white areas are unmelted tungsten and the energy density is listed as well as the unmelted tungsten percentage.

4.4 Hardness

The microhardness of the material was measured at room temperature and compared to other refractory high entropy alloys and refractory medium entropy alloys. It was found to be one of the highest values among these materials, as illustrated in Figure 4.10. The average microhardness was calculated for each sample across all three groups, as shown in Figure 4.11. Based on the results of the tungsten percentage and the microhardness values, it is evident that the most homogeneous sample, or the one with the least amount of unmelted tungsten, is the sample with laser parameters L2, represented by the purple bar in the graph. This suggests that these values might reflect the actual microhardness of the material. Even so, the average microhardness of 550 HV is one of the highest values compared to those reported in the literature, as seen in Figure 4.10.

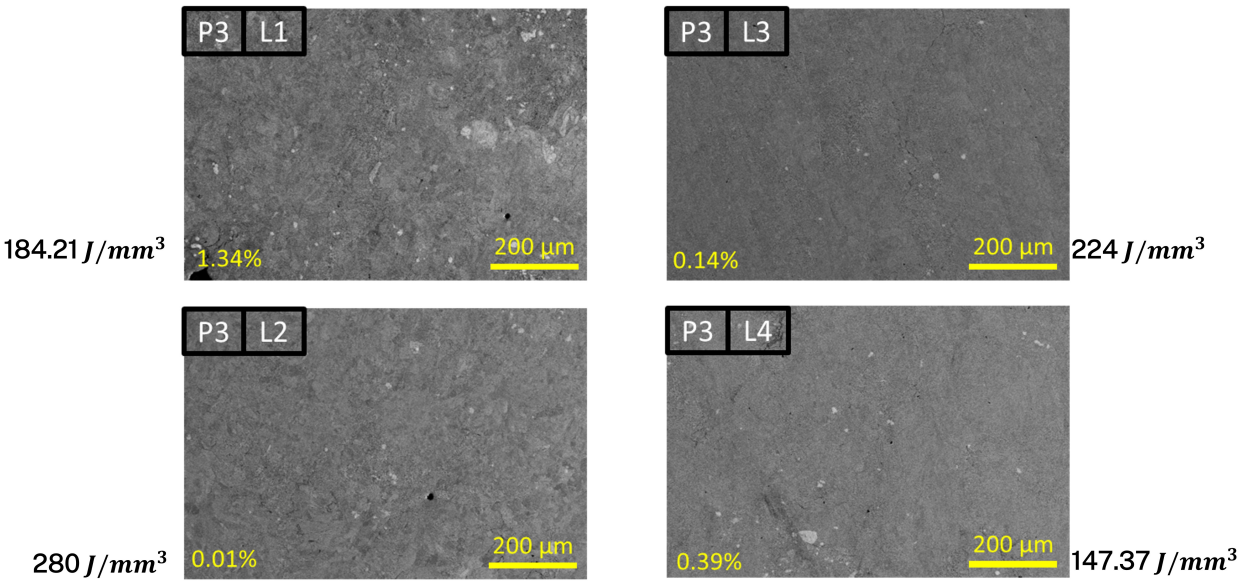

Figure 4.5: SEM of sample group 3. The white areas are unmelted tungsten and the energy density is listed as well as the unmelted tungsten percentage.

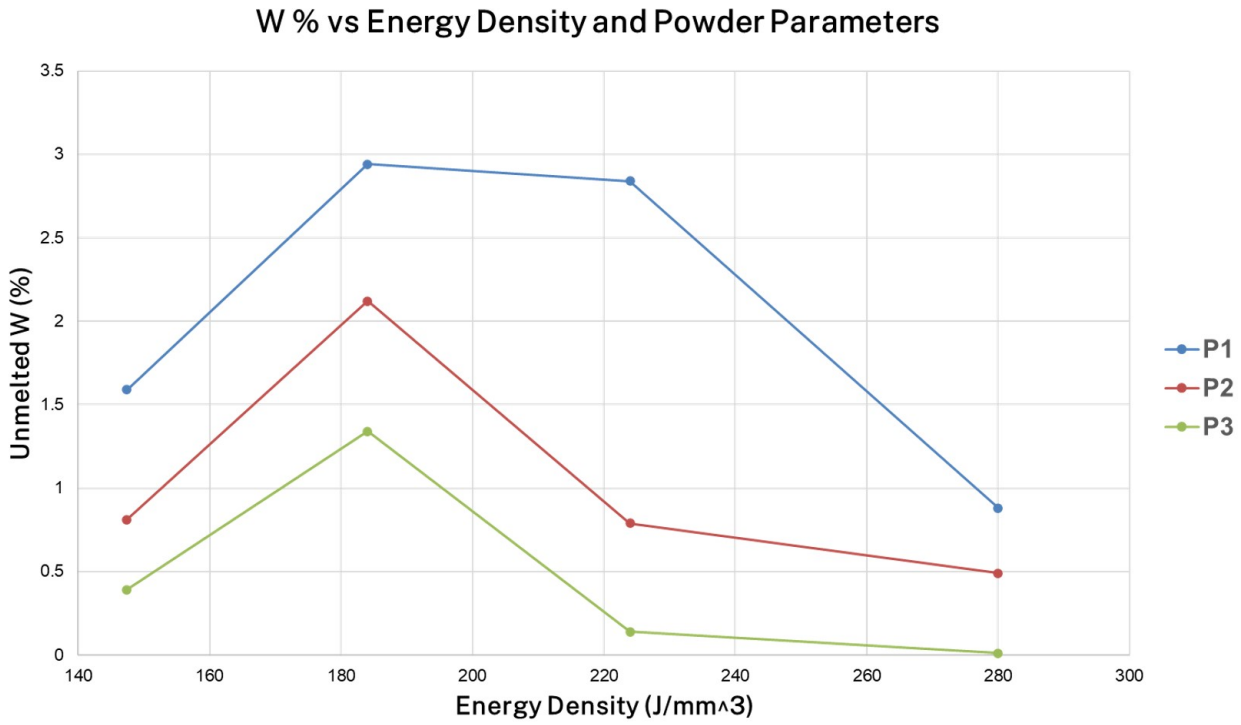

Figure 4.6: W% vs. Energy Density and Powder Parameters Graph.

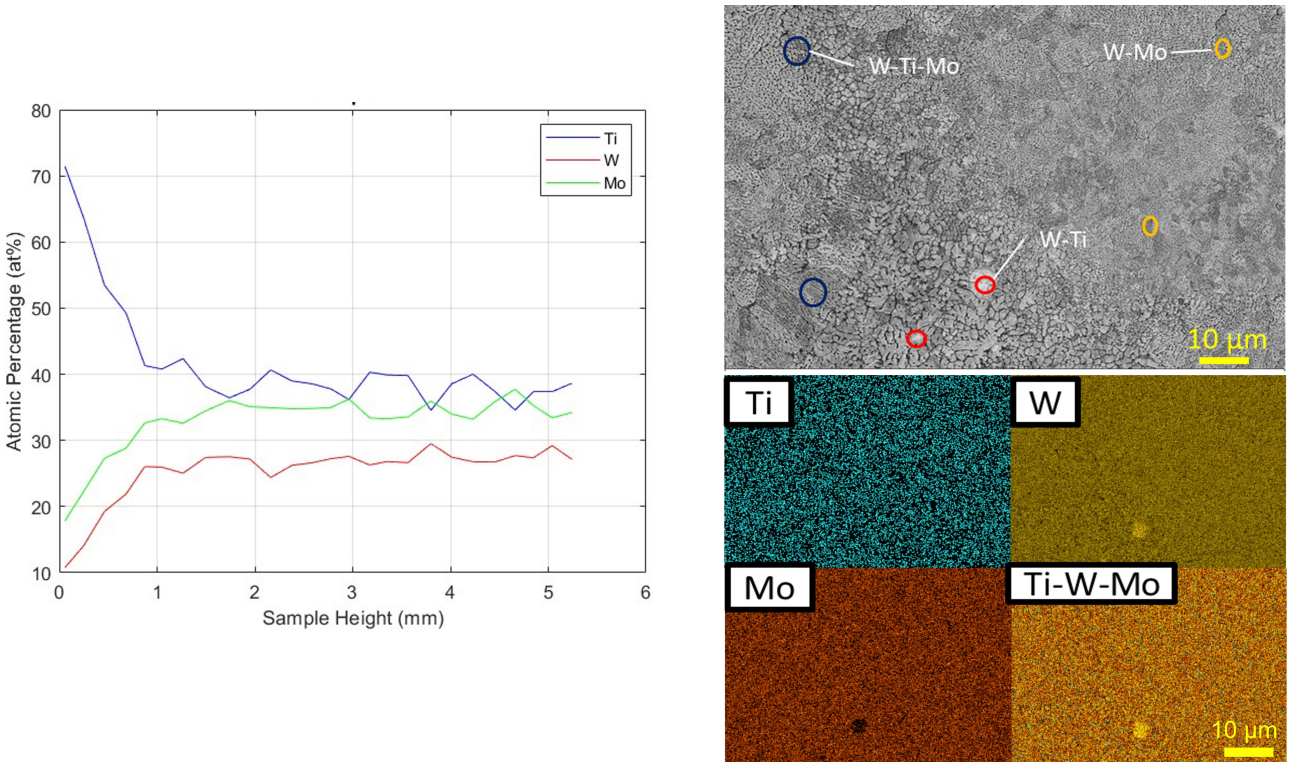

Figure 4.7: EDS analysis of TiWMo. The atomic percentage versus sample height are plotted from the interface of the sample all the way to the top of the sample, identification of microstructure based on the concentration of each element, and EDS mapping analysis.

$$VEC = \sum_{i=1}^{n} C_i (VEC)_i = 5.28$$

$$\Omega = \frac{T_m \Delta S_{mix}}{|\Delta H_{mix}|}, T_m = \sum_{i=1}^{n} C_i (T_m)_i = 1.9$$

$$\Delta H_{mix} = \sum_{i=1, i \neq j}^{n} 4 \Delta H_{ij} mix \; C_i C_j = -3.3$$

$$\Delta X = \sqrt{\sum_{i=1}^{n} C_i (x_i - \bar{x})^2}, \bar{x} = \sum_{i=1}^{n} C_i x_i = 2.02$$

$$\delta = \sqrt{\sum_{i=1}^{n} C_i \left(1 - \frac{r_i}{\bar{r}}\right)^2}, \bar{r} = \sum_{i=1}^{n} C_i r_i = 2.6\ \%$$

Figure 4.8: Phase Prediction Formulas

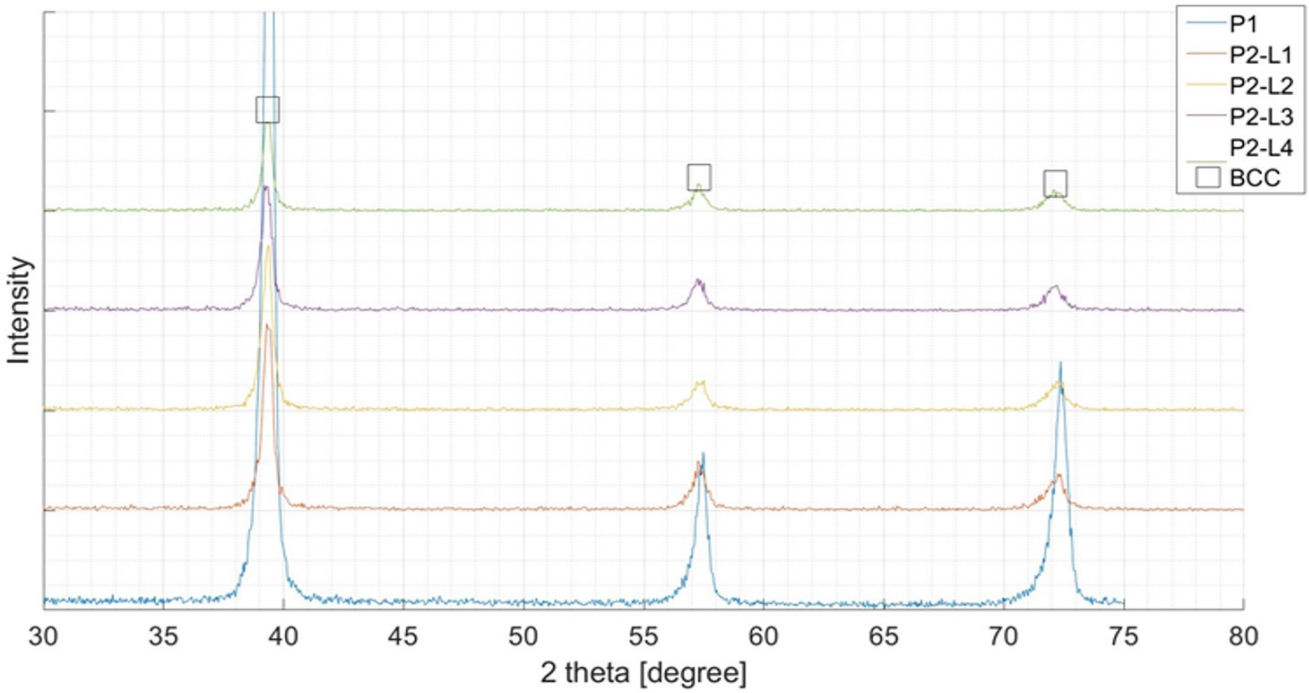

Figure 4.9: XRD plot showing a BCC phase formation.

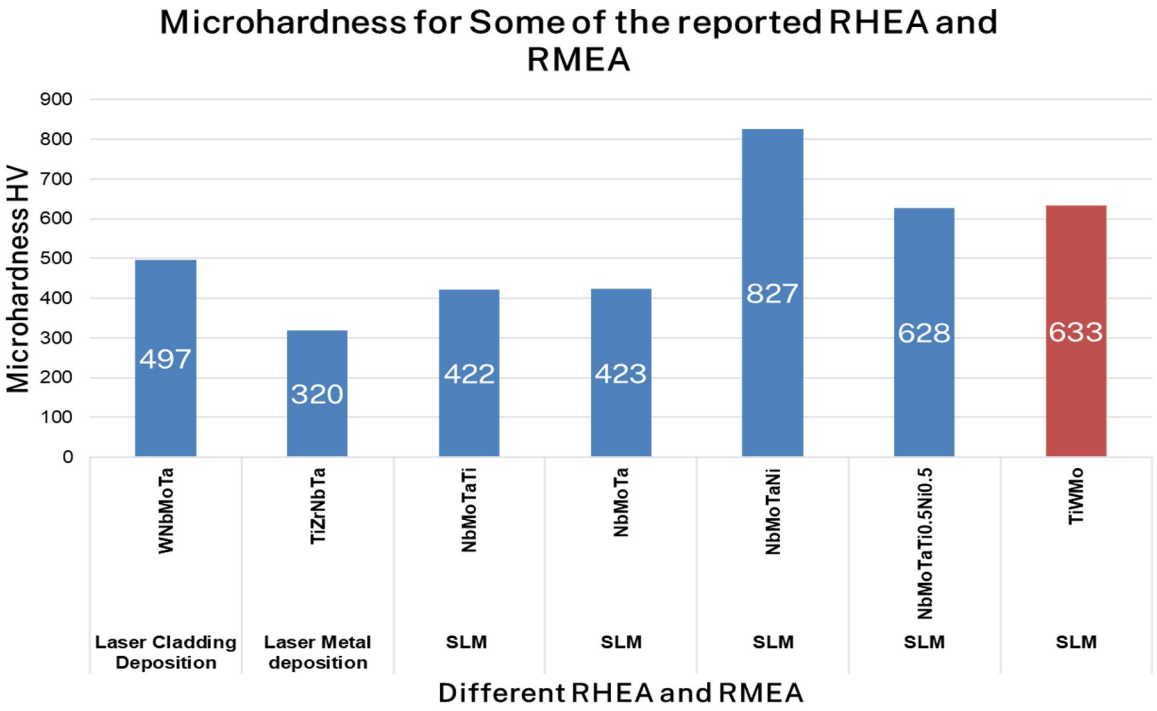

Figure 4.10: Microhardness of RHEA and RMEA found in the literature compared to the highest hardness values of TiWMo.

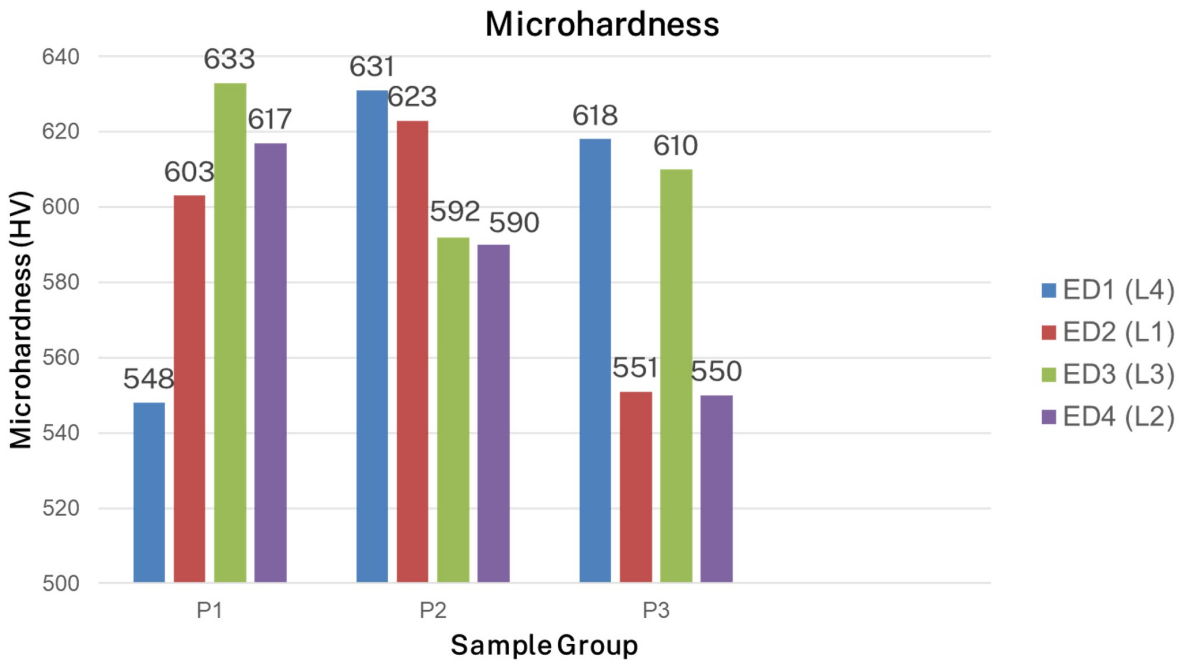

Figure 4.11: Microhradness graph of the average microhardness per sample per sample group.

CHAPTER V

CONCLUSION AND FUTURE WORK

Throughout this investigation, three sets of samples were produced using selective laser melting, with variations in laser power and scanning speed. The initial print involved a layer thickness and spherical particle size of 40 microns and 45 microns, respectively. The subsequent print incorporated a larger layer thickness of 50 microns, facilitating a broader melting pool. Irregular powder with a particle size of less than 35 microns was utilized in this second set. The third print was fabricated using tungsten powder with an irregular morphology and particle sizes ranging from 5 to 25 microns. The results show that a more homogeneous microstructure can be achieved by using irregularly shaped tungsten powder with smaller particle sizes. Specifically, utilizing a laser power of 350 watts and a scanning speed of 250 mm/s significantly reduced the percentage of unmelted tungsten particles to 0.01%.

In addition, compared to other alloys used for high-temperature applications, our material exhibits one of the highest microhardness values (HV) at room temperature, and we expect similar behavior at elevated temperatures. The research successfully demonstrated that using a titanium substrate in the powder bed fusion process is an effective method for producing refractory materials.

As part of the future research, the next phase will involve using spherical tungsten powder with particle sizes of $\leq$25 microns. By applying the parameters from the second print with this spherical powder, we aim to further enhance the flowability and layer packing density of the powder bed. This approach is expected to reduce the presence of unmelted tungsten particles and produce a high-quality, homogeneous Ti-Mo-W medium entropy alloy.

Additionally, we will conduct high-temperature microhardness and tensile tests to gain further insights into the mechanical properties of the refractory medium entropy alloy.

REFERENCES

[1] D. AQUARO AND M. PIEVE, *High temperature heat exchangers for power plants: Performance of advanced metallic recuperators*, Applied Thermal Engineering, 27 (2007), pp. 389–400.

[2] D. L. BOURELL, *Perspectives on additive manufacturing*, Annual Review of Materials Research, 46 (2016).

[3] M. BUZATU, Ş. I. GHICA, E. VASILE, V. GEANTĂ, R. ŞTEFĂNOIU, M. I. PETRESCU, G. IACOB, M. BUŢU, AND M. SOHACIU, *On the design of new β-phase titanium alloys ti-mo-w*, Univ. Politeh. Buchar. Sci. Bull. Ser. B, 78 (2016), pp. 161–172.

[4] B. DAS, V. SHARMA, K. S. S. MRUNAL, AND A. PATRA, *Microstructural and mechanical properties of ti-mo-w alloy by mechanical alloying and conventional sintering*, Materials Today: Proceedings, 27 (2020), pp. 1674–1680.

[5] S. FORD AND M. DESPEISSE, *Additive manufacturing and sustainability: an exploratory study of the advantages and challenges*, Journal of cleaner Production, 137 (2016), pp. 1573–1587.

[6] C. GADELMEIER, Y. YANG, U. GLATZEL, AND E. P. GEORGE, *Creep strength of refractory high-entropy alloy tizrhfnbta and comparison with ni-base superalloy cmsx-4*, Cell Reports Physical Science, 3 (2022).

[7] E. P. GEORGE, W. A. CURTIN, AND C. C. TASAN, *High entropy alloys: A focused review of mechanical properties and deformation mechanisms*, Acta Materialia, 188 (2020), pp. 435–474.

[8] C. HAASE, J. BÜLTMANN, J. HOF, S. ZIEGLER, S. BREMEN, C. HINKE, A. SCHWEDT, U. PRAHL, AND W. BLECK, *Exploiting process-related advantages of selective laser melting for the production of high-manganese steel*, Materials, 10 (2017), p. 56.

[9] Z. HAN, N. CHEN, S. ZHAO, L. FAN, G. YANG, Y. SHAO, AND K. YAO, *Effect of ti additions on mechanical properties of nbmotaw and vnbmotaw refractory high entropy alloys*, Intermetallics, 84 (2017), pp. 153–157.

[10] H. He, J. Wang, Y. Cao, X. Yang, G. Zhao, W. Yang, and J. Fang, *Effect of re and c on mechanical properties of nbtaw0. 4 refractory medium-entropy alloy at elevated temperature*, Journal of Alloys and Compounds, 931 (2023), p. 167421.

[11] H. Kim, Y. Lin, and T.-L. B. Tseng, *A review on quality control in additive manufacturing*, Rapid Prototyping Journal, 24 (2018), pp. 645–669.

[12] Y.-K. Kim, S. Yang, and K.-A. Lee, *Superior temperature-dependent mechanical properties and deformation behavior of equiatomic cocrfemnni high-entropy alloy additively manufactured by selective laser melting*, Scientific reports, 10 (2020), p. 8045.

[13] C. Liu, K. Zhu, W. Ding, Y. Liu, G. Chen, and X. Qu, *Additive manufacturing of wmotati refractory high-entropy alloy by employing fluidised powders*, Powder Metallurgy, 65 (2022), pp. 413–425.

[14] J. Man, B. Wu, G. Duan, L. Zhang, G. Wan, L. Zhang, N. Zou, and Y. Liu, *The synergistic addition of al, ti, mo and w to strengthen the equimolar cocrfeni high-entropy alloy via thermal-mechanical processing*, Journal of alloys and compounds, 902 (2022), p. 163774.

[15] J. K. Min, J. H. Jeong, M. Y. Ha, and K. S. Kim, *High temperature heat exchanger studies for applications to gas turbines*, Heat and mass transfer, 46 (2009), pp. 175–186.

[16] D. B. Miracle and O. N. Senkov, *A critical review of high entropy alloys and related concepts*, Acta Materialia, 122 (2017), pp. 448–511.

[17] A. O. Moghaddam, M. Sudarikov, N. Shaburova, D. Zherebtsov, V. Zhivulin, I. A. Solizoda, A. Starikov, S. Veselkov, O. Samoilova, and E. Trofimov, *High temperature oxidation resistance of w-containing high entropy alloys*, Journal of Alloys and Compounds, 897 (2022), p. 162733.

[18] S. Mooraj, X. Dong, S. Zhang, Y. Zhang, J. Ren, S. Guan, C. Li, R. Naorem, N. Argibay, W. Chen, et al., *Crack mitigation in additively manufactured al-crfe2ni2 high-entropy alloys through engineering phase transformation pathway*, Communications Materials, 5 (2024), p. 101.

[19] P. Niu, R. Li, K. Gan, T. Yuan, S. Xie, and C. Chen, *Microstructure, properties, and metallurgical defects of an equimolar cocrni medium entropy alloy additively manufactured by selective laser melting*, Metallurgical and Materials Transactions A, 52 (2021), pp. 753–766.

[20] S. QIU, G. ZHENG, AND Z. JIAO, *Alloying effects on phase stability, mechanical properties, and deformation behavior of cocrni-based medium-entropy alloys at low temperatures*, Intermetallics, 140 (2022), p. 107399.

[21] O. N. SENKOV, D. B. MIRACLE, K. J. CHAPUT, AND J.-P. COUZINIE, *Development and exploration of refractory high entropy alloys—a review*, Journal of materials research, 33 (2018), pp. 3092–3128.

[22] M.-H. TSAI AND J.-W. YEH, *High-entropy alloys: a critical review*, Materials Research Letters, 2 (2014), pp. 107–123.

[23] Y. WAN, Q. WANG, J. MO, Z. ZHANG, X. WANG, X. LIANG, AND B. SHEN, *Wretamo refractory high-entropy alloy with high strength at 1600° c*, Advanced Engineering Materials, 24 (2022), p. 2100765.

[24] F. WANG, T. YUAN, R. LI, S. LIN, Z. XIE, L. LI, V. CRISTINO, R. XU, AND B. LIU, *Comparative study on microstructures and mechanical properties of ultra ductility single-phase nb40ti40ta20 refractory medium entropy alloy by selective laser melting and vacuum arc melting*, Journal of Alloys and Compounds, 942 (2023), p. 169065.

[25] L. WANG, Y. FENG, Z. MAO, L. YANG, Y. XI, S. LI, D. YANG, J. JI, S. LEI, AND G. ZHANG, *Mechanical properties of a crconi medium entropy alloy in a gradient twin structure*, Journal of Materials Engineering and Performance, 31 (2022), pp. 7402–7411.

[26] M. WANG, R. LI, T. YUAN, C. CHEN, L. ZHOU, H. CHEN, M. ZHANG, AND S. XIE, *Microstructures and mechanical property of almgsczrmn-a comparison between selective laser melting, spark plasma sintering and cast*, Materials Science and Engineering: A, 756 (2019), pp. 354–364.

[27] S. XIN, M. ZHANG, T. YANG, Y. ZHAO, B. SUN, AND T. SHEN, *Ultrahard bulk nanocrystalline vnbmotaw high-entropy alloy*, Journal of Alloys and Compounds, 769 (2018), pp. 597–604.

[28] C. ZHANG, J. ZHU, H. ZHENG, H. LI, S. LIU, AND G. J. CHENG, *A review on microstructures and properties of high entropy alloys manufactured by selective laser melting*, International Journal of Extreme Manufacturing, 2 (2020), p. 032003.

[29] J. ZHANG, D. GU, Y. YANG, H. ZHANG, H. CHEN, D. DAI, AND K. LIN, *Influence of particle size on laser absorption and scanning track formation mechanisms of pure tungsten powder during selective laser melting*, Engineering, 5 (2019), pp. 736–745.

[30] J. ZHANG, B. SONG, Q. WEI, D. BOURELL, AND Y. SHI, *A review of selective laser melting of aluminum alloys: Processing, microstructure, property and developing trends*, Journal of Materials Science & Technology, 35 (2019), pp. 270–284.

VITA

Lindsey Salazar obtained her Bachelor of Science in Manufacturing Engineering from the University of Texas Rio Grande Valley in Dec 2021. She then continued her education and earned her Master of Science degree in Engineering Management from the University of Texas Rio Grande Valley in June 2024. During her academic career she was the first graduate student to participate as a guest researcher in the partnership with DEVCOM Army Research Laboratory in Additive Manufacturing. She can be reached at Lindseysalazar07@gmail.com.